An Ultra-Wideband Wire Spiral Antenna for In-Body Communications Using Different Material Matching Layers

Ali Khaleghi, Ilangko Balasingham, and Raúl Chávez-Santiago

***Abstract*—In this work an ultra-wideband wire antenna was designed and fabricated for transmitting/receiving signals to/from inside the human body. The antenna provides high gain and thus high field intensity in its broadside direction; hence, a high energy density wireless can be established with the inner body. The proposed antenna operates in the frequency band of 3-10 GHz with an impedance of 200 Ohms in free space. The antenna was embedded in different materials with permittivity values ranging from 12 to 74 in order to evaluate the matching layer effect on wave propagation from outside to inside the body. The antenna port impedance was adjusted by using matching circuits. The electric field intensity inside the human chest was calculated for different materials and depths. The best improvement in wave penetration was obtained for the frequency band of 750-1000 MHz by embedding the antenna inside a material with permittivity equal to 27.**

I. Introduction

The design of a compact antenna with a high-gain directive radiation pattern is required for a number of diagnostic and therapeutic applications in medicine based on the use of radio waves propagating into/from the human body. Examples of said applications are the communication interface of a wireless capsule endoscope (WCE) [1], medical radar for blood pressure estimation [2] and noninvasive imaging [3], and microwave hyperthermia for cancer treatment [4]. A properly designed antenna can transmit/receive to/from an implanted device over a significant part of the radio spectrum or transfer electromagnetic (EM) energy to internal organs. The main problem in these applications is, however, the high attenuation suffered by radio waves propagating in biological tissues. Therefore, it is desirable to improve the link quality of in-body radio links by reducing the path loss that may translate into better implant communication performance and higher resolution of radar or tomography images.

Ultra-wideband (UWB), as a new technology, has several potential applications in medicine [5]. By using UWB the data rate of an implantable communication system can increase, a microwave hyperthermia applicator can be focused more tightly, and a microwave imaging radar can provide higher quality images. A compact antenna design can allow sufficient space to install several antennas on the body surface thereby enabling spatial diversity or a phased array. Hence, the design of an efficient UWB antenna for in-body medical applications represents an important development.

A computational study of UWB wave propagation from outside to inside the body for the frequency ranges of 100-1000 MHz and 1-6 GHz was reported in [6]. A statistical model for UWB wave propagation into the body was introduced in [7], [8]. It has also been illustrated in [9] that by using different materials with different permittivity values around the body, i.e., a matching layer, the radio wave penetration inside the body can be improved by a factor of 5-10 depending on the matching material properties. These studies were conducted using a plane wave propagating into the chest.

In this paper the matching layer effect is analyzed by using a real antenna configuration in a wide frequency range. The proposed antenna design has an impedance of 30-60Ω depending on the surrounding materials. In free space it covers the frequency range of 3-10 GHz. The antenna was then embedded in different materials and placed near the body surface. When embedded in distilled water with permittivity equal to 74, the antenna covers the frequency range of 300-1000 MHz is covered when. This frequency range varies for different materials, but the common frequency range of 750-1000 MHz can be covered with high gain for materials with permittivity ranging from 12 up to 74. The proposed antenna has circular polarization at the main beam direction, thus the penetrating wave's polarization can be disregarded. The remainder of the paper is organized as follows. In section II, the antenna geometry and simulation parameters are described for the free space, and measurement and simulation results are provided. In section III, the simulation results of the antenna close to the body and embedded in different permittivity values are presented, where we provide the field intensity inside the human chest for different penetration depths. Section IV concludes this paper.

II. Antenna Design, Simulation and Measurement Results

The initial model of the antenna is a three dimensional dual Archimedean spiral wire antenna on top of a circular metal reflector of 80 mm in diameter. The parametric description of each branch of the spiral antenna is given as,

This work is part of the MELODY Project Phase II, which is financed by the Research Council of Norway under the contract no. 225885.

A. Khaleghi is with The Intervention Centre, Oslo University Hospital, 0272 Oslo, Norway (e-mail: ali.khaleghi@ rr-research.no). He is also with K. N. Toosi University of Technology, Iran.

I. Balasingham and R. Chávez-Santiago are with The Intervention Centre, Oslo University Hospital, Norway. They are also with the Institute of Clinical Medicine, University of Oslo, and the Department of Electronics and Communications, Norwegian University of Science and Technology (NTNU), Norway. (e-mails: ilangko.balasingham@medisin.uio.no; raul.chavez-santiago@rr-research.no).

978-1-4244-7929-0/14/$26.00 ©2014 IEEE

$$\begin{cases} x(t) = R \times t \times \sin(t)/(2\pi N) \\ y(t) = R \times t \times \cos(t)/(2\pi N) \\ z(t) = h \times t/(2\pi N) \\ 10 < t < 2\pi N \end{cases} \quad (1)$$

where R=20 mm is the base radius of the spiral, N=7 is the number of spiral turns, h=5 is the antenna height and t is a varying parameter. The wire diameter is 1.5 mm. Figure 1 shows the perspective view of the two spirals coiled 180° with respect to each other. The antenna at the apex forms a dipole configuration, which is fed by a balanced impedance matching unit. The impedance matching unit is in the form of a parallel plate transmission line that converts the coaxial unbalanced feed line to the balanced line at the dipole apex. The antenna is placed at a distance of 10 mm from the ground plane. The antenna matching with and without the metal reflector plate is almost the same, but the antenna gain with the reflector is larger than it is without it.

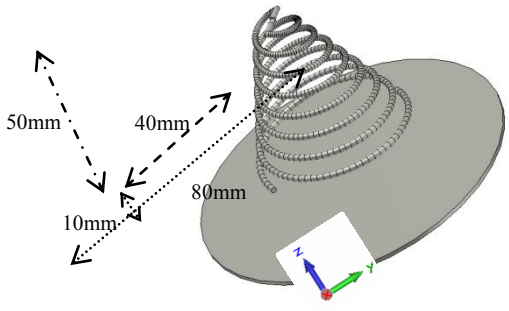

Fig. 1. Dual Spiral Archimedes antenna on top of a ground plane.

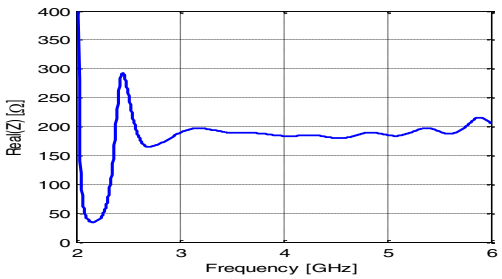

Fig. 2. Antenna impedance versus frequency in free space.

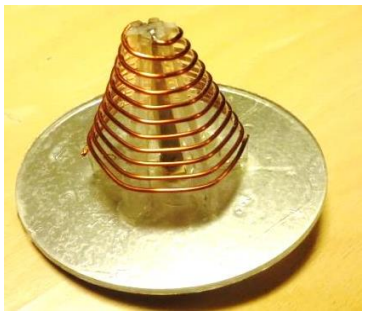

Fig. 3. Photography of the fabricated antenna and the matching unit.

The antenna parameters were optimized through numerical EM simulations using the finite-difference time-domain (FDTD) method to provide good impedance matching for the frequency range of 3-10 GHz. The simulated real part of the antenna impedance is shown in Fig. 2. An average impedance of 200Ω in the frequency range of 2.6-10 GHz can be observed. An antenna matching unit converts the 50Ω impedance of the SMA connector beneath the reflector to the 200Ω impedance of the antenna at the apex. Figure 3 shows the fabricated antenna with the matching unit.

The return loss and radiation patterns of the fabricated antenna were measured. Figure 4 shows the simulated and measured return loss versus frequency. As seen, the antenna has a return loss of less than 8 dB for the entire desired frequency band. The measurement and simulation results are in close agreement. The maximal far-field antenna gain is depicted in Fig. 5. As seen, the antenna gain varies within 4-7.5 dBi in the frequency range. The antenna radiation pattern was measured inside an anechoic chamber with far-field facility. The measured and simulated radiation patterns of the antenna for the E and H planes for the frequencies of 3, 4, and 5 GHz are shown in Fig. 6. Due to the antenna's directive pattern one can expect high near-field intensity in the broadside direction, which is desirable for in-body usage.

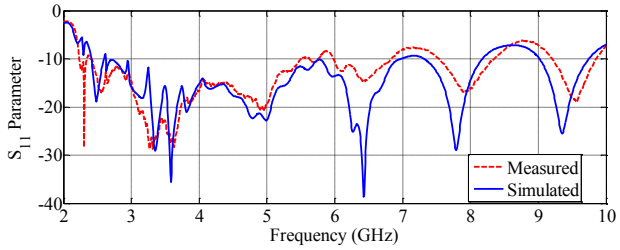

Fig. 4. Measured and simulated return loss for the antenna in free space with input impedance of 200Ω.

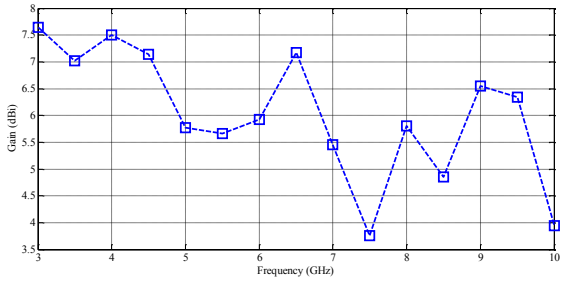

Fig. 5. Maximal gain of the fabricated antenna versus frequency.

III. Antenna Embedded in Different Materials in Proximity of the Body

Most wireless implantable medical devices operate in the narrowband frequency band of 401-405 MHz. The proposed antenna can cover this frequency range if it is embedded in an appropriate dielectric material. For this purpose the antenna was embedded in distilled water at 37°C with average permittivity of $\varepsilon_r = 74$. The dielectric constant of

water is frequency dependent. Taking this fact into account, the designed free-space antenna was simulated as if it were embedded in distilled water. From this simulation we can observe that the antenna's operating frequency range shifted to 300-1000 MHz with input impedance of 30Ω. A new impedance matching unit was needed to match the antenna characteristic impedance to the 50Ω impedance of the source. Figure 7 shows the simulated return loss versus frequency for the antenna embedded in distilled water. The radiation pattern of the embedded antenna for the new frequency range of 300-1000 MHz is directive, which makes the antenna more suitable for in-body application.

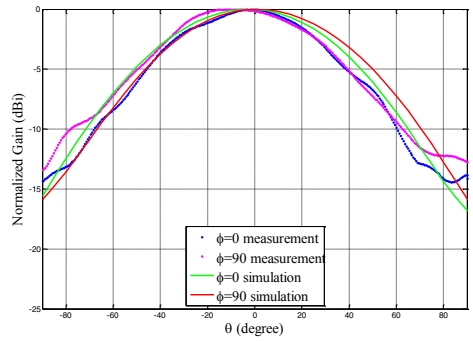

(a)

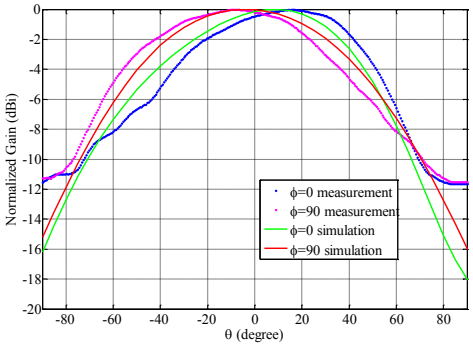

(b)

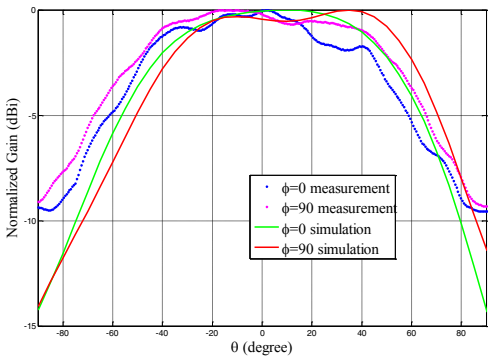

(c)

Fig. 6. Measured and simulated radiation pattern of the spiral antenna for the *E*-plane and *H*-plane at (a) 3 GHz, (b) 4 GHz, and (c) 5 GHz.

The antenna was also simulated as if it were embedded in different materials of permittivity equal to 12, 27, and 50. The corresponding port impedances varied within 40-60Ω. After matching the antenna, the computed return loss was obtained and is illustrated in Fig. 7. As seen, the operating frequency range varies in each case, but all the materials can provide good matching within 750-1000 MHz.

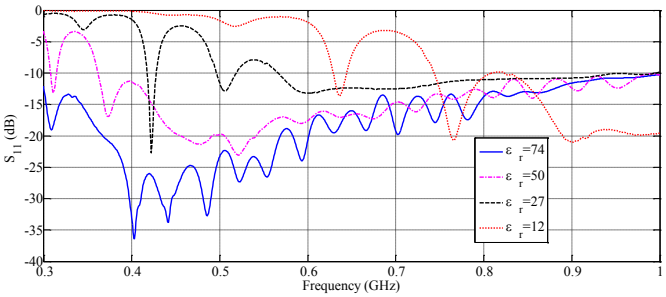

Fig. 7. Simulated return loss versus frequency of the antenna embedded in different materials, i.e., different permittivity values.

Then, the antenna embedded in different materials was placed at a distance of 4-5 from the human chest for numerical simulations. The main purpose was to evaluate the suitability of the different materials to function as a matching layer for the wave propagation into the body. A voxel anatomical model was used [6]. This human model includes different bilogical tissues with 32 assigned different frequency-dependant dielectric constants. The simulation scenario of the antenna close to the human body is illustrated in Fig. 8. The human torso with voxel resolution of 1 mm was employed, and 680 field probes for each component of E_x, E_z, were placed inside the chest in 8 different depth planes parallel to the surface. A depth resolution of 20 mm was considered and 85 probes were located on each plane. The 85 probes per plane were uniformly distributed in a rectangular shape that contained 17 probes in the *x*-direction and 5 probes in the *z*- direction with a resolution of 10 mm for each field component. The CST Microwave Studio™ platform was used for the numerical simulations. A Gaussian pulse was radiated and the field components inside the human tissues were computed. The frequency domain components of the penetrating wave at each probe position were obtained. The average (over 85 probes for a given depth) of the electric field intensity versus frequency was computed and the results are illustrated in Fig. 9 for each depth plane for the antenna embedded in distilled water. As seen, the field intensity diminishes as frequency increases due to the larger conductivity of the biological tissues at higher frequencies.

The overall average of the field intensity for the frequency range of 750-1000 MHz for each defined depth was obtained for the other matching layers. In this frequency range, the embedded antenna was properly matched in all the cases. Thus the impedance mismatch was removed from the results. Figure 10 shows the average electric field intensity for the *x*-axis component of the field. As seen, the electric field intensity is highest for the permittivity value of 27 in comparison to the other permittivity values. The wave penetration deteriorates above and below $\varepsilon_r = 27$. This

result is in agreement with simulations conducted using a plane wave instead of an antenna for different matching layers. The optimal matching permittivity of 27 can be explained by the varying dielectric properties of the human tissues arranged in a multilayer structure; these properties change depending on the water contents of each tissue.

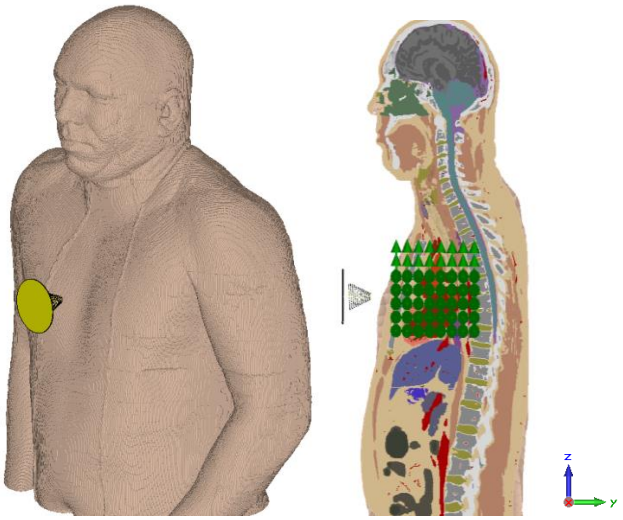

Fig. 8. Simulation scenario of the spiral antenna near an anatomical model. The field probes are also illustrated.

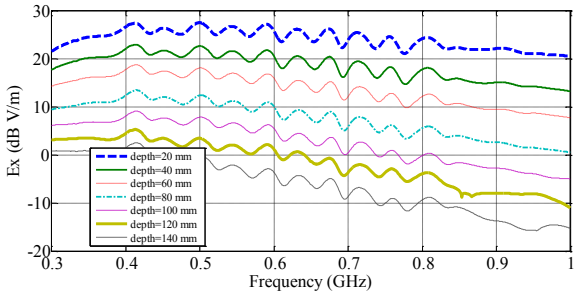

Fig. 9. Spectrum of the penetrating wave for different depths for the antenna embedded in distilled water with permittivity equal to 74.

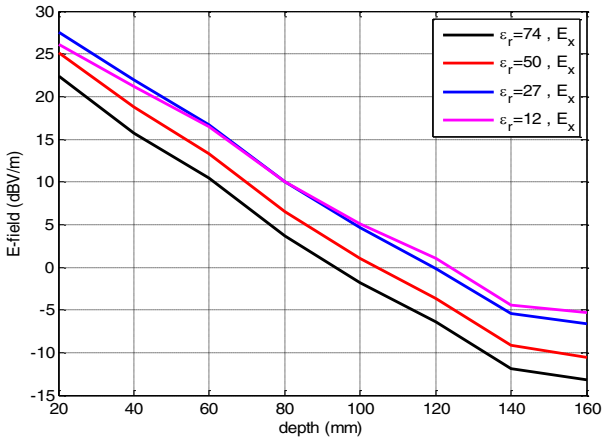

Figure 10. Average (over the frequency range of 750-1000 MHz) electric field intensity (dB V/m) inside the body versus depth.

In addition, we remark that the energy flow due to x-polarized and z-polarized electric field components are slightly different for low depth inside the body and are almost the same for deeper locations. Thus they have similar contribution to the energy transfer into the body. This is a direct result of the dual polarization of the antenna.

IV. Conclusion

A new design of an ultra-wideband spiral helical antenna was presented for biomedical applications. In free space, the antenna covers the frequency band of 3-10 GHz and provides a directive pattern with high field intensity in its aperture. If the antenna is embedded in distilled water then it can operate in 300-1000 MHz. In proximity of the human body, it was shown that a material with a permittivity value of 27 serves well as a matching layer providing the best wave penetration. A quantitative improvement of approximately 6 dB compared to the case of distilled water can be obtained. Although this study was conducted for the chest, the same procedure can be followed for the abdomen aimed at applications like wireless capsule endoscope communications. Similar results to those reported herein can be expected.

References

[1] R. Chávez-Santiago, and I. Balasingham, "The ultra wideband capsule endoscope," in *Proc. IEEE Intl. Conf. on Ultra-Wideband (ICUWB)*, Sydney, Australia, Sep. 15–18, 2013, pp. 72–78.

[2] L. E. Solberg, S. E. Hamran, T. Berger, and I. Balasingham, "Minimum variance signal selection for aorta radius estimation using radar," *EURASIP Journal on Advances in Signal Processing*, vol. 2010, no. 49, 2010.

[3] E. M. Staderini, "UWB radars in medicine," *IEEE Aerosp. Electron. Syst. Mag.*, vol. 17, no. 1, pp.13-18, Jan. 2002.

[4] M. Converse, E. J. Bond, B. D. Van Veen, and S. C. Hagness, "A computational study of ultra-wideband versus narrowband microwave hyperthermia for breast cancer treatment," *IEEE Trans. Microw. Theory Techn.*, vol.. 54, no. 5, pp. 2169-2180, May 2006.

[5] R. Chávez-Santiago, I. Balasingham, and J. Bergsland. (2012). Ultra wideband technology in medicine: A survey. *Journal of Electrical and Computer Engineering* [Online]. Vol. 2012, 9 pages. Available: http://www.hindawi.com/journals/jece/2012/716973/

[6] A. Khaleghi, I. Balasingham, and R. Chávez-Santiago, "Computational study of ultra-wideband wave propagation into the human chest," *IET Microwaves, Antennas & Propagation*, vol. 5, no. 5, pp. 559-567, Apr. 2011.

[7] A. Khaleghi, R. Chávez-Santiago, and I. Balasingham, "Ultra-wideband statistical propagation channel model for implant sensors in the human chest," *IET Microwaves, Antennas & Propagation*, vol. 5, no.15, pp. 1805-1812, December 2011.

[8] R. Chávez-Santiago, K. Sayrafian-Pour, A. Khaleghi, K. Takizawa, J. Wang, I. Balasingham, and H.-B. Li, "Propagation models for IEEE 802.15.6 standardization of implant communication in body area networks," *IEEE Commun. Mag.*, vol. 51, no. 8, pp. 80–87, Aug. 2013.

[9] A. Khaleghi, R. Chávez-Santiago, and I. Balasingham, "On the use of a dielectric matching layer for ultra wideband medical applications," in *Proc. 7th Intl. Conf. on Body Area Networks (BodyNets)*, Oslo, Norway, September 24-26, 2012, pp. 69-75.